IEEE Access
Multidisciplinary ⋮ Rapid Review ⋮ Open Access Journal

Received May 24, 2022, accepted June 14, 2022, date of publication June 20, 2022, date of current version June 24, 2022.

Digital Object Identifier 10.1109/ACCESS.2022.3184308

Wideband Bidirectional Same Sense Endfire Circularly Polarized Antenna

RAHUL KUMAR JAISWAL[1], (Member, IEEE), ANUJ KUMAR OJHA[1], KAHANI KUMARI[1], (Member, IEEE), KUMAR VAIBHAV SRIVASTAVA[1], (Senior Member, IEEE), AND CHOW-YEN-DESMOND SIM[2], (Senior Member, IEEE)

[1]Electrical Engineering Department, Indian Institute of Technology Kanpur, Kanpur 208016, India
[2]Electrical Engineering Department, Feng Chia University, Taichung 40724, Taiwan

Corresponding authors: Rahul Kumar Jaiswal (rahulgla2@gmail.com) and Chow-Yen-Desmond Sim (cysim@fcu.edu.tw)

This work was supported in part by the Ministry of Science and Technology (MOST), Taiwan, under Project MOST 110-2221-E-035-021; and in part by the Science and Engineering Research Board, India, under Project CRG/2021/000376.

ABSTRACT In this paper, a wideband bidirectional endfire circularly polarized (CP) antenna is proposed by combining two endfire CP antennas with a single coaxial probe feed. The wideband characteristics are achieved with the help of a two-layered substrate separated by an air gap, and the excitation of CP waves in the endfire directions is yielded by the wideband magnetic dipoles and tapered electric dipoles. The proposed CP antenna has shown wide 10-dB impedance bandwidth (IBW) and 3-dB axial ratio bandwidth (ARBW) of 20.76% (5.05 − 6.22 GHz) and 16.10% (5.14 − 6.04 GHz), respectively. Besides showing an overall size of $0.733\lambda_L \times 0.863\lambda_L \times 0.058\lambda_L$ (λ_L is the wavelength corresponding to the lowest operating frequency) with wide operational bandwidth, the proposed CP antenna has also demonstrated a desirable peak gain of 4.45 dBic.

INDEX TERMS Bidirectional, endfire circularly polarized antenna, same sense, wideband.

I. INTRODUCTION

The bidirectional antenna design has recently gained enormous attention in many applications such as long bridge/tunnel/coal mines communications [1], [2], radio frequency identification (RFID) systems [3], and various wireless communications systems. The bidirectional linearly polarized (LP) antennas have been reported in several papers [1], [2], [4]–[6], and amid these designs, the bidirectional LP antennas are successfully constructed using dipole array [1], [4], an array of rectangular rings [2], spoof surface plasmon polaritons [5], and slot with resonators [6].

The bidirectional CP antennas [3], [7]–[14] have various advantages over the bidirectional LP antenna type, such as orientation insensitive, better weather penetration, and interference reduction in the multipath environment. The bidirectional CP antenna can be mainly divided into two categories namely, broadside bidirectional CP antenna [3], [7]–[10], and endfire bidirectional CP antenna [11]–[14]. In [7] and [8], bidirectional CP with the same sense is achieved by the two-polarization conversion surface (coupling strip as mentioned in [8]) at the top and bottom of the microstrip fed slot antenna. The operating bandwidths of these polarization conversions surface-based bidirectional same sense CP antenna are 14.3% (5.2 − 6.0 GHz) [7] and 5.8% (2.33 – 2.47 GHz) [8]. Similarly, in [9], a polarization conversion surface is used on the top of the CP antenna to accomplish the same sense of circular polarization in both the top and bottom of the structure. Another way to realize the bidirectional CP antenna with the same sense is by using back-to-back slot coupled patches [10]. Even though good CP sense is achieved with the help of corner truncated patches, the operating bandwidth is only 0.81% (2.455 – 2.475 GHz).

Due to the continuous airflow ventilation in the coal mine tunnel, the endfire bidirectional antenna is a better candidate than the broadside bidirectional antenna because it provides a minimal cross-sectional area against the airflow [1]. Several bidirectional same sense endfire CP antennas have been reported in [11]–[14]. In [11], an array of crossed dipole and composite right/left-handed transmission lines (CRLH-TL) are applied, and the crossed dipole based bidirectional endfire CP antenna has an overall dimension of $0.717\lambda_L \times 0.446\lambda_L \times 0.446\lambda_L$ (λ_L is the wavelength corresponding to lowest operating frequency) and operating bandwidth is

The associate editor coordinating the review of this manuscript and approving it for publication was Chinmoy Saha.

limited by 11.8%. However, the above-reported literature shows that the endfire CP antenna profile is very large (3-Dimensional structure) and inappropriate for many applications. The bidirectional endfire CP antenna can be constructed using a back-to-back combination of the unidirectional endfire CP antenna. The unidirectional endfire CP antenna is formed by the combination of vertically polarized (VP) magnetic dipole and horizontally polarized (HP) electric dipole with a feed line [16]–[18]. The back-to-back combination of this unidirectional endfire CP antenna is used to form a bidirectional endfire CP antenna with the same sense as reported in [13]–[15]. The overall bandwidth of the bidirectional endfire CP antenna with same sense is 3.45% in [13], 2.93% in [14] and 2.8% in [15]. Therefore, the overall operational bandwidth of the above-reported antennas is limited, and it will not be suitable for wideband applications.

In this paper, a wideband bidirectional endfire same sense CP antenna is proposed. The bandwidth of the bidirectional endfire CP antenna is enhanced by combining the wideband bidirectional VP magnetic dipole with HP wideband electric dipoles. The operational bandwidths of both bidirectional magnetic dipole and electric dipole are further improved by implementing a two-layered structure with an air spacer. The overall 3-dB ARBW of the proposed bidirectional endfire CP antenna is 16.10% with the dimension of $0.733\lambda_L \times 0.863\lambda_L \times 0.058\lambda_L$. The proposed CP antenna is optimized using ANSYS Electronics Desktop (HFSS) and fabricated using the printed circuit board (PCB) method to verify the simulated predictions.

This manuscript is organized as follows. Firstly, the principle of operation for bidirectional endfire CP is investigated in section II, followed by studying the wideband VP magnetic dipole (unidirectional and bidirectional) in section III. Section IV describes the geometrical configuration of the proposed wideband bidirectional endfire CP antenna with experimental results. Finally, section V concludes the paper.

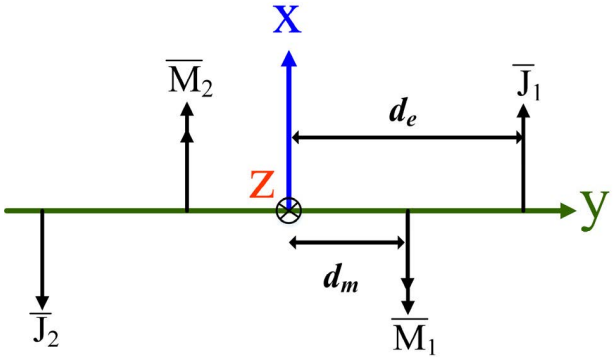

FIGURE 1. Orientation of electric and magnetic current source elements $\bar{J}$ and $\bar{M}$ for the bidirectional endfire CP antenna with same sense.

II. OPERATING PRINCIPLE OF BIDIRECTIONAL ENDFIRE CP ANTENNA WITH SAME SENSE

To generate a bidirectional endfire CP antenna with the same sense, an array of electric dipoles and magnetic dipoles are placed as shown in Fig. 1. Among two pairs of electromagnetic dipoles, one pair of the electric and magnetic dipoles is collocated along +x-direction, and the other pair is set along the -x-direction. The distance between the magnetic and electric dipole are $2d_m$ and $2d_e$, as illustrated in Fig. 1.

The total electric current ($\bar{J}$) is the sum of $\bar{J}_1$ and $\bar{J}_2$ and it can be written as

$$\bar{J} = \hat{a}_x J_{x0}\delta(x)\,\delta(y-d_e)\,\delta(z) - \hat{a}_x J_{x0}\delta(x)\,\delta(y+d_e)\,\delta(z) \tag{1}$$

Similarly, the total magnetic current ($\bar{M}$) is the sum of $\bar{M}_1$ and $\bar{M}_2$, and it can be stated as

$$\bar{M} = -\hat{a}_x M_{x0}\delta(x)\delta(y-d_m)\delta(z) + \hat{a}_x M_{x0}\delta(x)\delta(y+d_m)\delta(z) \tag{2}$$

where $\bar{J}_1 = -\bar{J}_2 = J_{x0}\hat{a}_x$ and $-\bar{M}_1 = \bar{M}_2 = M_{x0}\hat{a}_x$. Therefore, magnetic vector potential ($\bar{A}$) and electric vector potential ($\bar{F}$) due to these current sources can be expressed as

$$\bar{A} = \frac{\mu}{4\pi}\frac{e^{-jkr}}{r}(2j)\,[sin\,(kd_e \sin\theta sin\phi)]\,J_{x0}\hat{a}_x \tag{3}$$

$$\bar{F} = \frac{\varepsilon}{4\pi}\frac{e^{-jkr}}{r}(-2j)\,[sin\,(kd_m \sin\theta sin\phi)]\,M_{x0}\hat{a}_x \tag{4}$$

The total far-field electric field intensity along the +y-direction due to the above magnetic and electric vector potential can be specified as

$$\bar{E} = B\left[-\eta \sin(kd_e)\,J_{x0}\hat{a}_x + \sin(kd_m)\,M_{x0}\hat{a}_z\right] \tag{5}$$

where B is a constant. The condition for CP sense along the +y direction is expressed below

$$|\eta \sin(kd_e)\,J_{x0}| = |\sin(kd_m)\,M_{x0}| \tag{6}$$

and

$$(\angle \sin(kd_m)\,M_{x0}) - (-\angle \sin(kd_e)\,J_{x0}) = \begin{cases} +\left(\frac{1}{2}+2n\right)\pi\,RHCP \\ -\left(\frac{1}{2}+2n\right)\pi\,LHCP \end{cases} \tag{7}$$

Here, the distance between the electric current source and magnetic current source is $\lambda/4$ to get 90^0 phase differences. As two magnetic currents can be formed by using the back-to-back combination of half mode substrate integrated waveguide (HMSIW) [19], [20], the position of the magnetic current source (d_m) and electric current source (d_e) is set to be $\lambda/8$ and $3\lambda/8$ respectively, which play a vital role in obtaining the accurate dimension of the bidirectional magnetic dipole. Consequently, the modified magnitude condition is $\eta\,|J_{x0}| = |M_{x0}|$ while phase condition will remain the same as equation (7). Notably, analogous conditions will be obtained along the −y-direction accordingly. To further achieve wideband behavior for the bidirectional CP antenna with the same sense, the wideband bidirectional magnetic dipole and electric dipole are required. The electric dipole with wideband characteristics has been reported in many

papers, while there are limited papers available based on the wideband magnetic dipole. Therefore, a wideband magnetic dipole with unidirectional and bidirectional characteristic are investigated in subsequent sections.

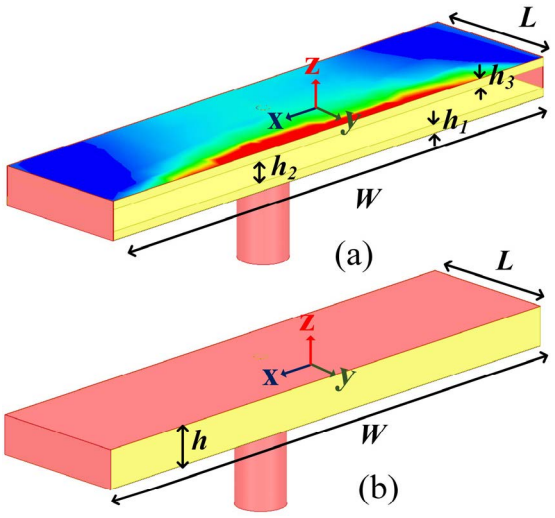

FIGURE 2. (a) Two-layered wideband unidirectional magnetic dipole with magnitude electric field(V/m) distribution on top surface (b) single-layered wideband unidirectional magnetic dipole (design parameters specifications in mm: $W = 53$, $L = 17$, $h_1 = 0.8$, $\varepsilon_{r1} = 4.4$, $h_2 = 2.0$, $\varepsilon_{r2} = 1.0$, $\varepsilon_{r3} = 4.4$, $h_3 = 0.8$, $h = 3.6$).

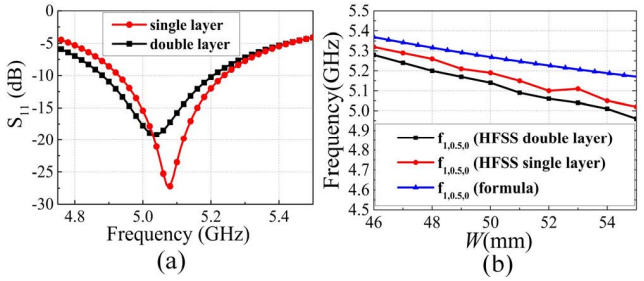

FIGURE 3. (a) Simulated S-parameter response of single and double-layered unidirectional magnetic dipole. (b) variation of the resonance frequency of the dominant mode ($TE_{1,0.5,0}$) with width (W) of the single and double-layered cavity.

III. WIDEBAND VERTICALLY POLARIZED MAGNETIC DIPOLE

A. WIDEBAND UNIDIRECTIONAL MAGNETIC DIPOLE

The half mode substrate integrated waveguide (HMSIW) is used to form a vertically polarized (VP) unidirectional magnetic dipole. To reduce the complexity, shorting walls on the three sides are used to prevent leakage instead of vias [18], as depicted in Fig. 2. Here, a double-layered HMSIW is designed by implementing two FR4 substrates ($\varepsilon_r = 4.4$, $\tan\delta = 0.02$) each with a thickness of 0.8 mm separated by an air gap of 2 mm, as shown in Fig. 2(a). The quasi $TE_{1,0.5,0}$ is the dominant mode in the HMSIW [13], and it can be verified by observing the magnitude of electric field (V/m) distribution on the top surface of the two-layered cavity, as shown in Fig. 2(a). The equivalent dielectric constant of the two layered-cavity can be calculated by using equation (8) [21].

$$\varepsilon_{eq} = \frac{h}{\frac{h_1}{\varepsilon_{r1}} + \frac{h_2}{\varepsilon_{r2}} + \frac{h_3}{\varepsilon_{r3}}} \tag{8}$$

$$f_r = \frac{1}{2\sqrt{\mu\varepsilon}}\sqrt{\left(\frac{1}{W}\right)^2 + \left(\frac{0.5}{L}\right)^2} \tag{9}$$

Here, the calculated equivalent dielectric constant is obtained as 1.523. To verify the antenna design, the equivalent dielectric constant (ε_{eq}) is taken as 1.523, and the height of the substrate 'h' is the summation of h_1, h_2, and h_3. Therefore, the single-layered magnetic dipole is constructed by taking a single dielectric constant of $\varepsilon_{eq} = 1.523$ and height $h = 3.6$ mm, as shown in Fig. 2(b). The reflection coefficient curve for both single and double-layered unidirectional magnetic dipole is shown in Fig. 3(a). It reveals that both the structure provides a similar response with IBW of around 6%. However, lowering the profile of the similar unidirectional magnetic dipole delivers lesser IBW, and for the given thickness of 0.8 mm, it provides only 1.9% of IBW. The resonance frequency of the dominant mode of both single and double-layered with respect to width (W) of the cavity is plotted in Fig. 3(b). The resonance frequency of the dominant mode can also be calculated by using equation (9) [13], and Fig. 3(b) shows the frequency plot for different widths. It can be observed that all three curves are in good agreement with each other. Therefore, the above-mentioned equations are valid to calculate the dimension of the HMSIW-based magnetic dipole.

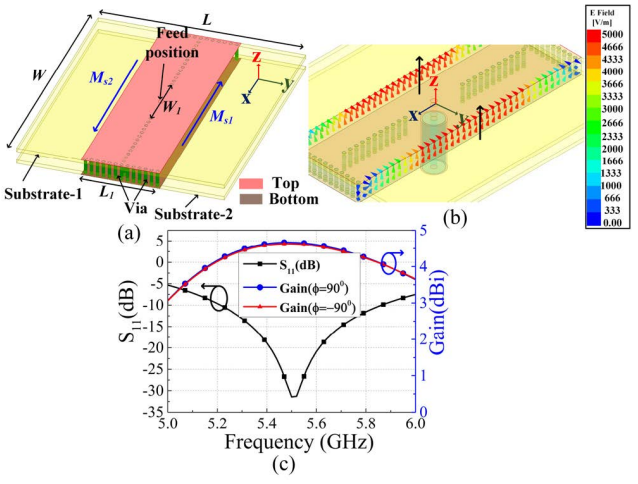

FIGURE 4. (a) Wideband bidirectional magnetic dipole (isometric view). (b) electric field distribution on open aperture. (c) simulated reflection coefficient and gain response of wideband bidirectional magnetic dipole with design parameters (in mm): $W = 53$, $L = 45$, $L_1 = 17$, $W_1 = 13.6$.

B. WIDEBAND BIDIRECTIONAL MAGNETIC DIPOLE

The VP bidirectional magnetic dipole can be constructed by exciting the two magnetic current sources on the open aperture, as shown in Fig. 4(a). The back-to-back combination of the HMSIW constructs the two-element array of the magnetic dipole. The electric field distribution on the open aperture is illustrated in Fig. 4(b). As the direction of the electric field

on the open aperture is the same (+ z-direction), and outward unit normal vectors on these apertures are in opposite directions, these magnetic current sources are in the opposite direction, as shown in Fig. 4(a). Here, the single feed mechanism is applied instead of using two separate feeds to excite the two magnetic dipoles. The feeding location and the gap (W_1) within the shorting wall are decided by the good matching condition of the antenna element. The simulated reflection coefficient curve and the gain curve are depicted in Fig. 4(c). Here, it can be observed that the resonance frequency of this magnetic dipole is dependent on the length L_1, width W, and the opening space of W_1. The same phenomenon can be well observed in Fig. 2, as discussed above. The proposed two-layered magnetic dipole alone provides IBW of 11.7%, with a peak realized gain of 4.5 dBi. The simulated 2D radiation patterns plotted across the two principal planes (xy and yz plane) are shown in Figs. 5(a) and (b), respectively. It can be observed that the E_θ component is a co-polarized radiation pattern in the endfire direction. Along the $\theta = 0^0$, a null can be observed due to equal and opposite magnetic dipoles, which are symmetrically placed with respect to the center of the antenna.

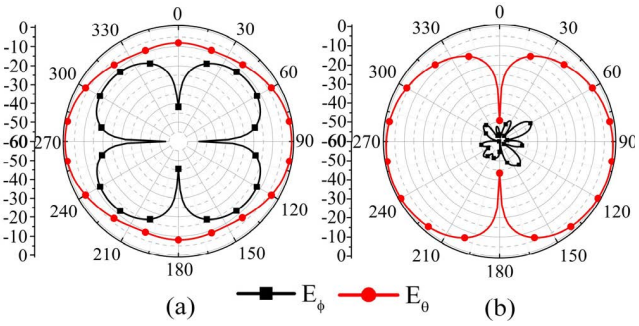

FIGURE 5. Simulated 2D radiation pattern of a wideband bidirectional magnetic dipole in (a) xy plane (b) yz plane at 5.5 GHz.

Consequently, these magnetic dipoles are combined with the two electric dipoles (collocated along the x-direction) with λ/4 feed length, and a good CP wave will be achieved with endfire direction. Since the x-directed electric dipole exhibits an E_ϕ component as the co-polarized radiation pattern along the y-direction, the conditions to achieve CP wave will be satisfied when two orthogonal components E_θ (magnetic dipole) and E_ϕ(electric dipole), will become equal in magnitude and have 90^0 phase difference. Therefore, to achieve a bidirectional endfire CP antenna, the magnetic dipole loaded with a pair of electric dipoles will be investigated in the next section.

IV. WIDEBAND BIDIRECTIONAL ENDFIRE CIRCULARLY POLARIZED ANTENNA WITH SAME SENSE

A. ANTENNA DESIGN

The schematic diagram and fabricated structure of the proposed wideband endfire CP antenna are shown in Figs. 6 and 7, respectively. The proposed structure is printed on the top layer of substrate-1 and the bottom layer of substrate-2. Both substrates are made of FR4 dielectric sheet ($\varepsilon_r = 4.4$, $\tan\delta = 0.02$) with a thickness of 0.8 mm. The bidirectional magnetic dipole is formed at the open aperture of the cavity, as discussed earlier in section III. This cavity can be considered as the back-to-back combination of the HMSIW. The two-layered back-to-back combination of the HMSIW is constructed by applying vias along the two side edges (along the y-direction) and along the centerline (along the x-direction), as shown in Fig. 6(a). Since the proposed antenna is a double-layered PCB (printed circuit board) structure, conventional vias formation cannot be implemented. Therefore, these vias are implemented using copper wire of diameter 0.6 mm, bypassing it through each hole and followed by proper soldering connection at both top and bottom layer, as shown in Fig. 7. Proper soldering is required to get a proper connection with printed copper metal and vias.

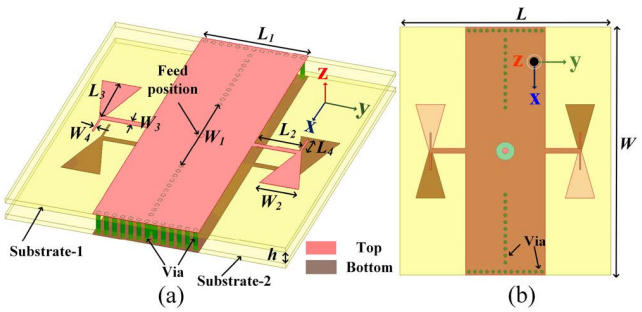

FIGURE 6. Schematic diagram of proposed wideband bidirectional endfire CP antenna with same sense. (a) isometric view. (b) top view with the design parameters. $W = 53$, $L = 45$, $L_1 = 17$, $L_2 = 7.3$, $L_3 = 10.0$, $L_4 = 3.4$, $W_1 = 18.6$, $W_2 = 6.3$, $W_3 = 1.0$, $W_4 = 0.3$, $h = 2$, via diameter = 0.6, via spacing = 1.45 (in mm).

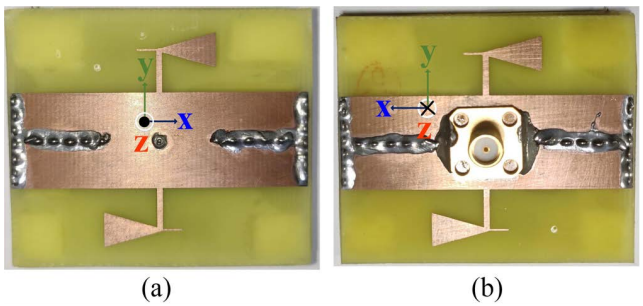

FIGURE 7. Fabricated structure of proposed wideband bidirectional endfire CP antenna with same sense, (a) top view, (b) bottom view.

To get a bidirectional endfire CP wave, tapered electric dipoles are placed on both sides of the magnetic dipole but in the reverse direction. The straight feed line is used to connect the magnetic and electric dipoles. A 50 Ω coaxial connector is connected at the centre to excite the wideband bidirectional endfire CP antenna. The opening space (W_1) and overlapping edge at shorter width of the electric dipole of length (L_4) are very significant parameters to yield good impedance matching as well as axial ratio bandwidth (ARBW).

B. RESULT AND ANALYSIS

The proposed wideband bidirectional endfire CP antenna with the same sense is optimized and analyzed using ANSYS Electronics Desktop (HFSS). To validate the simulated

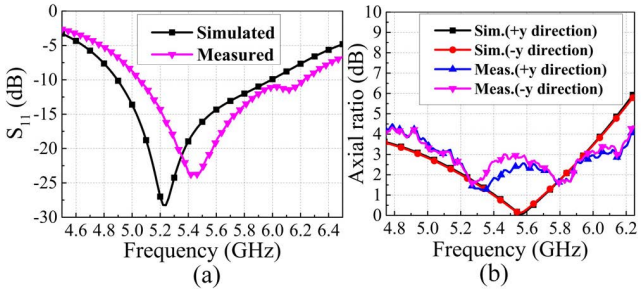

FIGURE 8. Simulated and measured results of the proposed wideband bidirectional endfire CP antenna. (a) reflection coefficient curve (b) axial ratio curve.

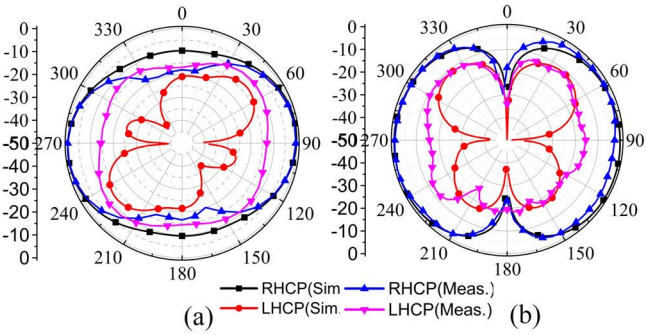

FIGURE 9. Simulated and measured radiation pattern in (a) xy plane, (b) yz plane at 5.5 GHz.

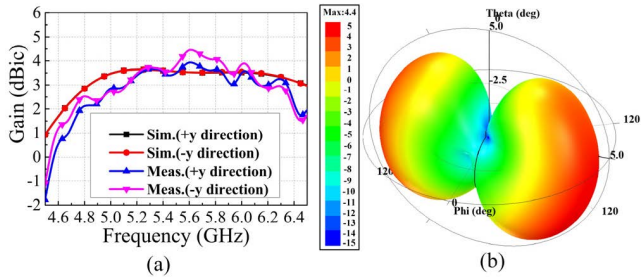

FIGURE 10. (a) Simulated and measured total realized gain curves (b) 3D radiation pattern at 5.5 GHz of the proposed endfire CP antenna.

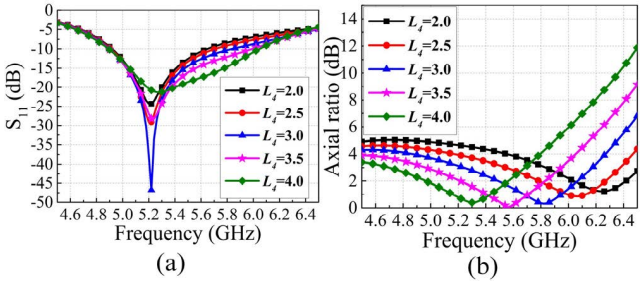

FIGURE 11. Effects of L_4 on (a) reflection coefficient curve, (b) axial ratio curve of proposed wideband bidirectional endfire CP antenna.

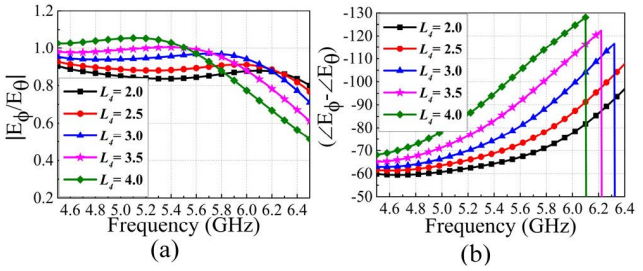

FIGURE 12. Effects of L_4 on (a) $\left|\frac{E_\Phi}{E_\theta}\right|$, (b) $\angle E_\Phi - \angle E_\theta$ of proposed wideband bidirectional endfire CP antenna along +y direction.

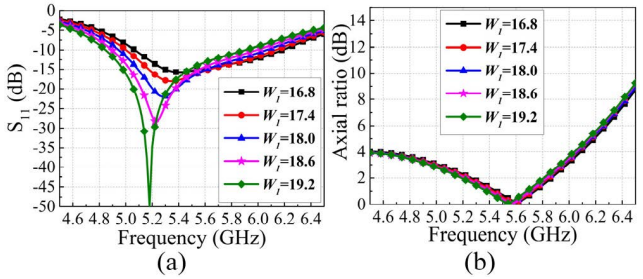

FIGURE 13. Effects of W_1 on (a) reflection coefficient curve, (b) axial ratio curve of proposed wideband bidirectional endfire CP antenna.

results, the prototype of the antenna model was fabricated using printed circuit board (PCB) technology, as shown in Fig. 7. The simulated reflection coefficient and axial ratio curve are shown in Figs. 8(a) and (b), respectively. The reflection coefficient is measured using the N5222A PNA network analyzer (Agilent Technologies), and the far-field parameters are measured in a standard Anechoic Chamber. It can be observed that the simulation results are in good agreement with the measured ones.

The simulated 10-dB bandwidth (or IBW) and 3-dB ARBW (or CP bandwidth) of the proposed CP antenna are 20.22% (4.89 − 5.99 GHz) and 17.95% (4.97 − 5.95 GHz), respectively, while its corresponding measured ones are 20.76% (5.05 − 6.22 GHz) and 16.10% (5.14 − 6.04 GHz), respectively. Fig. 9 shows the simulated and measured radiation patterns of the endfire CP antenna in two principal planes. It is observed that the right hand circularly polarized (RHCP) radiation is along the endfire directions. The simulated polarization purity along the endfire direction is better than 40 dB at the centre frequency. The measured co-polarized radiation pattern is well matched with the simulated co-polarized radiation pattern. The deviation in cross-polarization is observed due to the higher value of the axial ratio at the centre frequency, as observed in the measured axial ratio diagram shown in Fig. 8(b). The simulated and measured gain plot of the endfire CP antenna is illustrated in Fig. 10(a). The proposed antenna provides a peak gain of 4.45 dBic in the endfire direction. Due to the combined effect of fabrication intolerances and material imperfections, slight deviations are observed in the measured responses. The 3D radiation pattern is depicted in Fig. 10(b), and it confirms that the proposed CP antenna has bidirectional endfire characteristics.

To better comprehend the wideband bidirectional endfire CP antenna, the effects of tuning the antenna parameters length L_4 and the opening space W_1 have been analyzed through the parametric analysis, as shown in Figs. 11 to 13.

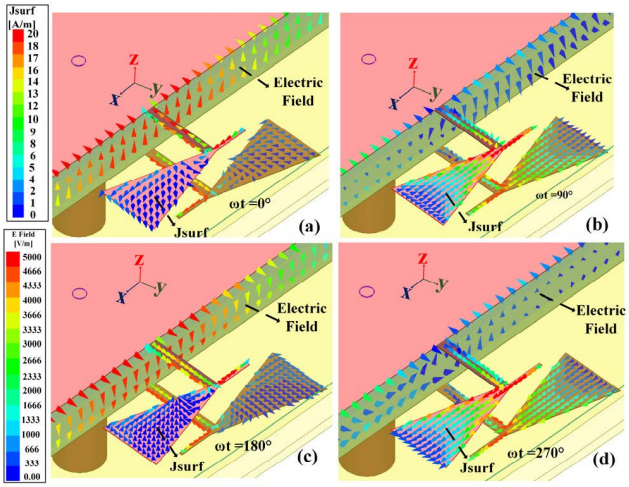

FIGURE 14. Electric field and surface current distribution (solid line) on the open aperture and tapered electric dipole, respectively, with different time instant at ωt = (a) 0^0, (b) 90^0, (c) 180^0, and (d) 270^0, at 5.5 GHz.

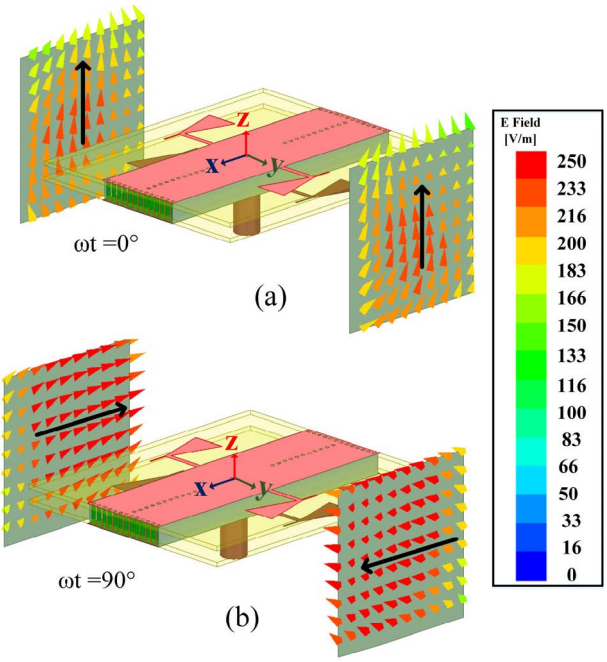

FIGURE 15. Vector electric field distribution of the proposed bidirectional endfire CP antenna for two different instants of time, (a) $\omega t = 0^0$ and (b) $\omega t = 90^0$, at 5.5 GHz.

In Fig. 11(a), as L_4 increases from 2.0 mm to 4.0 mm (with a step increment of 0.5 mm), a minimal variation in the resonance frequency is observed. In contrast, the axial ratio curve shifted towards the lower frequency, as shown in Fig. 11(b). Therefore, the length L_4 can be used to tune the axial ratio without affecting the reflection coefficient curve. The effect of length L_4 on the ratio of the magnitude of orthogonal electric field ($\left|\frac{E_\Phi}{E_\theta}\right|$) and phase difference ($\angle E_\Phi - \angle E_\theta$) of the proposed wideband bidirectional endfire CP antenna along the +y direction is depicted in Fig. 12. It can be observed that when $L_4 = 3.5$ mm, a good AR performance is achieved. Similarly, the opening space W_1 is another significant parameter to yield good impedance matching without affecting the axial ratio curve, as shown in Fig. 13. Here, when $L_4 = 3.5$ mm and $W_1 = 18.6$ mm, good IBW and ARBW can be achieved. For the visualization of CP wave generated by the combination of orthogonal components (electric dipole and magnetic dipole), the electric field distribution on the open aperture and electric field distribution away from the antenna are presented in Figs. 14 and 15, respectively.

The electric field and surface current distribution on the open aperture and tapered electric dipole, respectively, with different time instant (ωt), are depicted in Fig. 14. For time instant $\omega t = 0^0$, the magnitude of the electric field on the open aperture is high, and a small magnitude of surface current distribution on the electric dipole is observed. On the other hand, at $\omega t = 90^0$, a low electric field appears on the open aperture, and the electric dipole has shown high surface current distribution. Therefore, it is confirmed that there is an approximately 90^0 phase difference between the electric and magnetic dipole. Furthermore, the sense of polarization can be identified by Fig. 15 for both endfire directions. At time instant $\omega t = 0^0$, the electric field is directed along the +z-direction at both ends. For $\omega t = 90^0$, the polarization of the electric field is along the +x-direction and −x-direction for +y and −y directed CP wave, respectively. Similarly, for $\omega t = 180^0$ and 270^0, they have followed the same trend. Therefore, the proposed wideband bidirectional endfire CP antenna with the same sense provides the RHCP polarization for both endfire directions.

TABLE 1. Comparison with other bidirectional ENDFIRE CP antenna with the same sense.

Reference	IBW (%)	ARBW (%)	Dimension (λ_L^3)	Peak gain (dBic)
[12]	30.2	7.8	0.486× 0.486 × 0.915	3.80
[13]	3.45	3.45	1.626× 1.291 × 0.028	4.85
[14]	2.9	2.9	0.610× 0.500 × 0.029	1.42
[15]	2.8	>2.8	0.523× 0.467 × 0.029	4.04
Proposed work	**20.76**	**16.1**	**0.733× 0.863 × 0.058**	**4.45**

IBW: Impedance bandwidth, ARBW: Axial ratio bandwidth, λ_L: wavelength corresponding to lowest operating frequency

Table 1 shows the performance comparison between the proposed wideband bidirectional CP antenna and those (with the same sense) reported in [12]–[15]. Notably, limited literature is available for bidirectional endfire CP antenna with the same sense. In [12], the overall operating bandwidth is only 7.8% with the very large antenna profile. Therefore, it can be realized that the proposed antenna provides a wider IBW (at least six times higher) and ARBW (more than four times) with a comparative antenna profile with respect to the other reported literature. Furthermore, it has also exhibited decent gain characteristics without any additional director or array implementation. Nevertheless, it is noteworthy that the gain of this proposed endfire CP antenna can be further enhanced by considering low loss substrate, implementing additional

directors at the front of the antenna, or arranging it as an array but at the cost of a larger size.

V. CONCLUSION

A wideband bidirectional endfire CP antenna with the same sense has been successfully designed theoretically and experimentally validated with a fabricated prototype. The bidirectional magnetic dipole was realized by a back-to-back combination of HMSIW, while the bidirectional magnetic dipoles and tapered electric dipoles are connected via a feed line to yield a desirable CP wave in the endfire direction. The significant enhancement of the proposed antenna in the overall ARBW (16.10%) with overlapped IBW of 20.76% was achieved by using two-layered configurations. The measured peak gain of this endfire CP antenna was 4.45 dBic. Due to the above-mentioned antenna performances, the proposed wideband bidirectional endfire CP antenna with the same sense can be used in long tunnels or coal mines to improve security where wideband characteristics are required.

REFERENCES

[1] L. Liu, Z. Zhang, Z. Tian, and Z. Feng, "A bidirectional endfire array with compact antenna elements for coal mine/tunnel communication," *IEEE Antennas Wireless Propag. Lett.*, vol. 11, pp. 342–345, 2012.

[2] W. Liu, Z. Zhang, Z. Tian, and Z. Feng, "A bidirectional high-gain cascaded ring antenna for communication in coal mine," *IEEE Antennas Wireless Propag. Lett.*, vol. 12, pp. 761–764, 2013.

[3] Y. F. Lin, H. M. Chen, F. H. Chu, and S. C. Pan, "Bidirectional radiated circularly polarised square-ring antenna for portable RFID reader," *Electron. Lett.*, vol. 44, no. 24, pp. 1383–1384, Nov. 2008.

[4] H. Guo and W. Geyi, "Design of bidirectional antenna array with adjustable endfire gains," *IEEE Antennas Wireless Propag. Lett.*, vol. 18, no. 8, pp. 1656–1660, Aug. 2019.

[5] D. Tian, R. Xu, G. Peng, J. Li, Z. Xu, A. Zhang, and Y. Ren, "Low-profile high-efficiency bidirectional endfire antenna based on spoof surface plasmon polaritons," *IEEE Antennas Wireless Propag. Lett.*, vol. 17, no. 5, pp. 837–840, May 2018.

[6] J.-F. Qian, F.-C. Chen, K.-R. Xiang, and Q.-X. Chu, "Resonator-loaded multi-band microstrip slot antennas with bidirectional radiation patterns," *IEEE Trans. Antennas Propag.*, vol. 67, no. 10, pp. 6661–6666, Oct. 2019.

[7] N. Hussain, S. I. Naqvi, W. A. Awan, and T. T. Le, "A metasurface-based wideband bidirectional same-sense circularly polarized antenna," *Int. J. RF Microw. Comput.-Aided Eng.*, vol. 30, no. 8, 2020, Art. no. e22262.

[8] J. Wu, R. Lian, Z. Wang, and Y. Yin, "Strip-coupling circularly polarized antenna and its same-sense bidirectional array," *J. Electromagn. Waves Appl.*, vol. 29, no. 14, pp. 1859–1866, Sep. 2015.

[9] F. Khosravi and P. Mousavi, "Bidirectional same-sense circularly polarized slot antenna using polarization converting surface," *IEEE Antennas Wireless Propag. Lett.*, vol. 13, pp. 1652–1655, 2014.

[10] Y. Hou, Y. Li, L. Chang, Z. Zhang, and Z. Feng, "Bidirectional same-sense circularly polarized antenna using slot-coupled back-to-back patches," *Microw. Opt. Technol. Lett.*, vol. 59, no. 3, pp. 645–648, Mar. 2017.

[11] W. Liu, Z. Zhang, and Z. Feng, "A bidirectional circularly polarized array of the same sense based on CRLH transmission line," *Prog. Electromagn. Res.*, vol. 141, pp. 537–552, 2013.

[12] Y. Zhao, K. Wei, Z. Zhang, and Z. Feng, "A waveguide antenna with bidirectional circular polarizations of the same sense," *IEEE Antennas Wireless Propag. Lett.*, vol. 12, pp. 559–562, 2013, doi: 10.1109/LAWP.2013.2259462.

[13] J. Hu, Z.-C. Hao, K. Fan, and Z. Guo, "A bidirectional same sense circularly polarized endfire antenna array with polarization reconfigurability," *IEEE Trans. Antennas Propag.*, vol. 67, no. 11, pp. 7150–7155, Nov. 2019.

[14] Y. Yan, Y. Jiao, and C. Zhang, "A circularly polarized-reconfigurable planar end-fire antenna with bidirectional radiation of same sense and wide beamwidth," *Int. J. RF Microw. Comput.-Aided Eng.*, vol. 30, no. 12, Dec. 2020, Art. no. e22469.

[15] M. Ye, X.-R. Li, and Q.-X. Chu, "Single-layer single-fed endfire antenna with bidirectional circularly polarized radiation of the same sense," *IEEE Antennas Wireless Propag. Lett.*, vol. 16, pp. 621–624, 2017.

[16] R. K. Jaiswal, K. Kumari, C. Sim, and K. V. Srivastava, "Three-port circularly polarized MIMO antenna for WLAN application with pattern and polarization diversity," *Microw. Opt. Technol. Lett.*, vol. 63, no. 7, pp. 1927–1934, Jul. 2021.

[17] W.-H. Zhang, W.-J. Lu, and K.-W. Tam, "A planar end-fire circularly polarized complementary antenna with beam in parallel with its plane," *IEEE Trans. Antennas Propag.*, vol. 64, no. 3, pp. 1146–1152, Mar. 2016.

[18] W. Zhou, J. Liu, and Y. Long, "A broadband and high-gain planar complementary Yagi array antenna with circular polarization," *IEEE Trans. Antennas Propag.*, vol. 65, no. 3, pp. 1446–1451, Mar. 2017.

[19] W. Hong, B. Liu, Y. Wang, Q. Lai, H. Tang, X. X. Yin, Y. D. Dong, Y. Zhang, and K. Wu, "Half mode substrate integrated waveguide: A new guided wave structure for microwave and millimeter wave application," in *Proc. Joint 31st Int. Conf. Infr. Millim. Waves 14th Int. Conf. Teraherz Electron.*, Sep. 2006, p. 219.

[20] Q. Lai, C. Fumeaux, W. Hong, and R. Vahldieck, "Characterization of the propagation properties of the half-mode substrate integrated waveguide," *IEEE Trans. Microw. Theory Techn.*, vol. 57, no. 8, pp. 1996–2004, Aug. 2009.

[21] K. Dutta, D. Guha, C. Kumar, and Y. M. M. Antar, "New approach in designing resonance cavity high-gain antenna using nontransparent conducting sheet as the superstrate," *IEEE Trans. Antennas Propag.*, vol. 63, no. 6, pp. 2807–2813, Jun. 2015.

RAHUL KUMAR JAISWAL (Member, IEEE) received the B.Tech. degree in electronics and communication engineering from Uttar-Pradesh Technical University, Lucknow, India, in 2012, and the M.Tech. degree in microwave electronics from the University of Delhi South Campus, Delhi, India, in 2016. He is currently pursuing the Doctor of Philosophy (Ph.D.) degree in RF and microwaves discipline with the Electrical Engineering Department, Indian Institute of Technology Kanpur, India, under the supervision of Prof. Kumar Vaibhav Srivastava. He worked as a Project Trainee with the Society for Applied Microwave Electronics Engineering and Research (SAMEER), Kolkata, from 2015 to 2016. He worked as a Scientist with the Institute for Plasma Research (IPR), Gandhinagar, India, from 2016 to 2017. He has published several journals/conference papers on various aspects of antennas and RF waveguides. His research interests include MIMO antennas, circularly polarized antennas, unidirectional and bidirectional endfire CP antennas, base station antennas, and full-duplex antennas. He received the IEEE Antennas and Propagation Society Doctoral Research Grant in 2021. He is also serving as the Chair for the IEEE APS-SBC, IIT Kanpur.

ANUJ KUMAR OJHA received the M.Tech. degree in digital communication from Rajasthan Technical University (RTU), Kota, Rajasthan, in 2013, and the Ph.D. degree from the Department of Electrical and Electronics Engineering, Birla Institute of Technology and Science, BITS Pilani, (Pilani Campus), Rajasthan, India, in 2020. His thesis was on the Performance Enhancement of Cylindrical Dielectric Resonator Antennas for Low Cross Polarization and High Gain Applications. He worked as a Project Fellow with the MEMS Group, CSIR-CEERI Pilani, Rajasthan, from 2013 to 2015, where he worked on the development of silicon-based MEMS piezoresistive pressure sensors for various applications. He is currently working as a Research Associate with the Department of Electrical Engineering, Indian Institute of Technology Kanpur, Uttar Pradesh, India. He has published several journals/conference papers on various aspects of MEMS sensors, dielectric resonator antennas, and RF sensors. His research interests include dielectric resonator antennas, higher-order mode antennas, sensors, filtering antennas, metamaterial absorbers, and MIMO antennas.

KAHANI KUMARI (Member, IEEE) received the B.Tech. degree in electronics and communication engineering from the West Bengal University of Technology, Kolkata, India, in 2012, and the M.E. degree in microwave communication from the Indian Institute of Engineering Science and Technology, Shibpur, India, in 2015. She is currently pursuing the Doctor of Philosophy (Ph.D.) degree in RF and microwaves discipline with the Electrical Engineering Department, Indian Institute of Technology (IIT) Kanpur, India. She has published several journals/conference papers on various aspects of full-duplex antennas and circularly polarized antennas. Her research interests include full-duplex antennas, MIMO antennas, circularly polarized antennas, unidirectional and bidirectional endfire CP antennas, and base station antennas.

KUMAR VAIBHAV SRIVASTAVA (Senior Member, IEEE) received the B.Tech. degree in electronics engineering from the Kamla Nehru Institute of Technology, Sultanpur, India, in 2002, and the M.Tech. and Ph.D. degrees in electrical engineering from the Indian Institute of Technology Kanpur (IIT Kanpur), Kanpur, India, in 2004 and 2008, respectively. He was with the GE Global Research Centre, Bengaluru, India, for one year in 2008. In 2009, he joined the Department of Electrical Engineering, IIT Kanpur, as an Assistant Professor, where he has been working as a Professor, since November 2018. He has published more than 115 international journal articles, two international patents, and 150 conference papers in the last 15 years. His research interests include microwave antennas, metamaterials, metamaterial absorbers and cloaking, FDTD technique, and MIMO antennas. He received various national and best paper awards. He was the Chairperson of the IEEE UP Section, in 2018, and the Founding Chair of the IEEE Antenna and Propagation Society Chapter in UP Section.

CHOW-YEN-DESMOND SIM (Senior Member, IEEE) was born in Singapore, in 1971. He received the B.Sc. degree from the Engineering Department, University of Leicester, U.K., in 1998, and the Ph.D. degree from the Radio System Group, Engineering Department, University of Leicester, in 2003. From 2003 to 2007, he was an Assistant Professor with the Department of Computer and Communication Engineering, Chienkuo Technology University, Changhua, Taiwan. In 2007, he joined the Department of Electrical Engineering, Feng Chia University (FCU), Taichung, Taiwan, as an Associate Professor, where he became a Full Professor, in 2012, and as a Distinguish Professor, in 2017. He worked as the Executive Officer of Master's Program with the College of Information and Electrical Engineering (Industrial Research and Development) and the Director of the Intelligent IoT Industrial Ph.D. Program, from August 2015 to July 2018. He co-founded the Antennas and Microwave Circuits Innovation Research Center, FCU, and worked as the Director, from 2016 to 2019. Since October 2016, he has been serving as the Technical Consultant for Securitag Assembly Group (SAG), which is one of the largest RFID tag manufacturers in Taiwan. He has been serving as the Consultant for Avary (the largest PCB manufacturer in mainland China), since August 2018. He worked as the Head of the Department of Electrical Engineering, FCU, from August 2018 to July 2021. He has authored or coauthored over 180 SCI articles. His current research interests include antenna design, VHF/UHF tropospheric propagation, and RFID applications. He is a fellow of the Institute of Engineering and Technology (FIET), a Senior Member of the IEEE Antennas and Propagation Society, and a Life Member of the IAET. He has served as the TPC member for many international conferences. He was a recipient of the IEEE Antennas and Propagation Society Outstanding Reviewer Award (IEEE TRANSACTIONS ON ANTENNAS AND PROPAGATION) for eight consecutive years from 2014 to 2021. He has also received the Outstanding Associate Editor Award from the IEEE ANTENNAS WIRELESS AND PROPAGATION LETTERS in July 2018. He has served as the TPC Sub-Committee Chair (Antenna) for the ISAP 2014 and PIERS 2017/2019. He has served as the Advisory Committee for InCAP 2018/2019 and ICoICCS 2021, and has also served as the TPC Chair for the APCAP 2016 and iWEM 2019/2020, and the Track Chair for ICCC 2022. He was the General Co-Chair of ISAP 2021. He has served as the Chapter Chair for the IEEE AP-Society, Taipei Chapter, from January 2016 to December 2017. He was the Founding Chapter Chair of the IEEE Council of RFID, Taipei Chapter, from October 2017 to December 2020. He was invited as the Workshop/Tutorial Speaker of APEMC 2015, iAIM 2017, and InCAP 2018, and the Invited Speaker of TDAT 2015, iWAT 2018, APCAP 2018, ISAP 2019, InCAP 2019, ISRAST 2020, ISAP 2020, URSI GASS 2021, iWEM 2021, WAMS 2022, and ISAP 2022. He was the Keynote Speaker of SOLI 2018 and NEAST 2020. He has served as the AE for IEEE ACCESS from August 2016 to January 2021. He is also serving as an Associate Editor for the IEEE ANTENNAS AND WIRELESS PROPAGATION LETTERS, the IEEE JOURNAL OF RADIO FREQUENCY IDENTIFICATION, and *International Journal of RF and Microwave Computer-Aided Engineering* (Wiley).